

Sedimentary characteristics of the Lower Cambrian Niutitang shale in the southeast margin of Sichuan Basin, China



Jun Liu ^a, Yanbin Yao ^{a,*}, Derek Elsworth ^b, Zhejun Pan ^c, Xiaoxiao Sun ^a, Weihua Ao ^a

^a Coal Reservoir Laboratory of National Engineering Research Center of CBM Development & Utilization, China University of Geosciences, Beijing 100083, PR China

^b Department of Energy and Mineral Engineering, Pennsylvania State University, University Park, PA 16802, USA

^c CSIRO Energy Flagship, Private Bag 10, Clayton South 3169, Australia

ARTICLE INFO

Article history:

Received 14 December 2015

Received in revised form

22 March 2016

Accepted 29 March 2016

Available online 19 April 2016

Keywords:

Gas shale

Niutitang formation

Sedimentary pattern

Southeast margin of Sichuan basin

ABSTRACT

The Lower Cambrian Niutitang formation shale in the Sichuan Basin is not only a source rock for the Sinian conventional gas reservoir but also a possible reservoir for shale gas. However, very limited work have been focused on the detailed sedimentary environment related to shale gas exploration. In this study, detailed field geological investigation, continuous sampling and analyses by SEM, EDS XRD, XRF and ICP-OES, were used to probe provenance and sedimentary environment of the Niutitang formation shale in the southeast margin of Sichuan Basin. Both field outcrop observation and laboratory experimental results indicate: 1) the presence of framboidal pyrite; 2) $\delta\text{U} \geq 1$; and 3) a negative δCe index anomaly. The detrital mineral properties and major element analyses indicate that the geotectonic background of the sediment sources for the Niutitang formation shale can be linked to the neritic zone and slope zone. The horizontal bedding indicates that suspended sediments were involved in the sedimentation. The Ba minerals, REE characteristics and trace element index (U/Th) demonstrate that most of the study area was formed in a normal sedimentary environment, but several isolated zones were affected by submarine hydrothermal sedimentation. The sedimentation of the Niutitang shale most likely occurred in a weak hydrodynamic, deep water, oxygen-deficient reducing environment. The major sediment sources were continental margins, such as the neritic and continental slope zones.

© 2016 Elsevier B.V. All rights reserved.

1. Introduction

Shale gas exploration and production have received increased interest due to the growing global energy demand (Johnson and Boersma, 2013). Organic-rich black shales are considered the source rocks or seals for most conventional oil and gas reservoirs (Arthur and Sageman, 1994). Meanwhile, shale is also characterized as a self-contained source rock-reservoir system, in which hydrocarbon fluids are derived from solid organic matter through biogenic and/or thermogenic processes (Crutis, 2002; Hill et al., 2007a).

Commercial shale gas production began in the United States and was enabled by the key technical developments of horizontal drilling and massive hydraulic fracturing (Crutis, 2002; Jarvie et al., 2007). Presently, unconventional shale gas represents a key

resource in the United States and has surpassed natural gas production from non-shale sources (Energy Information Administration [EIA], 2014). Large-scale shale gas utilization and development have drastically fulfilled the worldwide energy supply (Jarvie et al., 2007). Shale gas has attracted significant public attention in countries other than the USA (Crutis, 2002; Chalmers et al., 2012), such as Australia, Canada, Germany and China.

China possesses abundant shale gas resources. Commercial shale gas production has recently begun at a few shale gas fields, among which the Jiaoshiba shale gas field in the southeastern Sichuan Basin has been the most successful (Wu et al., 2013; Yang et al., 2015; Chen et al., 2015a,b). The first shale gas well in the Jiaoshiba gas field, the JY1HF well, yielded a shale gas flow of $20.3 \times 10^4 \text{ m}^3/\text{day}$ (7.2 mmcf/day) in 2012. The JY8-2HF well has a peak production rate of $54.7 \times 10^4 \text{ m}^3/\text{day}$ (19.4 mmcf/day) (Chen et al., 2015a,b). The target shale gas production seam in the Jiaoshiba gas field is the lower Silurian Longmaxi marine shale. In addition to the Longmaxi formation, the Lower Cambrian Niutitang formation (also called the Qiongzhusi Formation) is another thick

* Corresponding author.

E-mail address: yyb@cugb.edu.cn (Y. Yao).

and continuous marine shale (Zhang et al., 2008).

In the southeastern Sichuan Basin, the thickness of the Niutitang formation shale (simplify as Niutitang shale in the following text) ranges from 20 to 100 m, with the maximum thickness in the southeast margin of Sichuan Basin (Fig. 1a; Nie et al., 2011; Xie et al., 2013), where the shale has high TOC, high thermal maturity and large gas-in-place (Huang et al., 2012; Xie et al., 2013). All these properties suggest a potential target area for shale gas production. There are some researches related to the sedimentary and tectonic framework of the southeastern Sichuan Basin, and the analyses of the geochemical and physical characteristics of the Niutitang shale in Sichuan basin. For example, Zeng et al. (2016) investigated the development characteristics of three types of natural fractures in the Paleozoic marine shales of the southeastern Sichuan Basin. Xue et al. (2016) investigated the relationship between TOC and pore development characteristics of the Niutitang shale in Sichuan Basin. However, due to limited exploration data, the detailed discussion about the petrological, mineralogical and geochemical characteristics and the sedimentary environment of the Niutitang formation shale are not yet available for the southeastern Sichuan Basin.

In this study, we performed field geological investigation of fresh sedimentary outcrops, then performed petrological, mineralogical and geochemical analyses on shale samples in laboratories, and finally provided some new evidence to explain the detailed sedimentary characteristics of the Niutitang shale. This study is useful to better understand the origin of shale gas, and petrological and physical properties of the Lower Cambrian Niutitang formation gas shale in the study area.

2. Geological setting

The southeast Sichuan Basin covers southern Chongqing, northern Guizhou and southeastern Sichuan, among which the study area belongs to southeastern Chongqing City. Tectonically, the study area is located at the southeast margin of the southeastern Sichuan Basin (Fig. 1). The southeast Sichuan Basin is composed of S–N and NE–SW trending fold belts and fault zones (Fig. 1). Caledonian movement led to the stratigraphic lacuna of the Devonian and Carboniferous Systems, except from the Neoproterozoic Sinian, Paleozoic and Mesozoic systems in the study area (Reinhardt, 1988; Hao et al., 2013; Jiang et al., 2013; Zeng et al., 2016) (Fig. 2). Among these sedimentary strata, there are four sets of hydrocarbon source rocks, including the Lower Cambrian Niutitang shale, Upper Ordovician-Lower Silurian Wufeng-Longmaxi shale, Lower Permian carbonate source rocks and Upper Permian coal-bearing shale (Fig. 2). These shales, which are widely distributed with great thickness and high pyrite, organic matter and biological fossil contents, are the prior targets for the exploration and development of Paleozoic marine shale gas in southern China (Wang et al., 2009 and Dong et al., 2010; Zeng et al., 2016).

The Niutitang shale is conformably overlain by the grayish-green shale, mudstone and silty mudstone of the Lower Cambrian Mingxinsi formation. Meanwhile, a parallel unconformity exists between the Niutitang formation and the underlying Upper Sinian Dengying formation (Fig. 2).

3. Sampling and experiments

3.1. Samples

Fifteen shale groups were sampled from the southeast margin of Sichuan Basin. The locations of sampling are shown in Fig. 1b). Fresh samples were collected directly from outcrops or geological

profiles of the Niutitang formation, with a block sample size of $10 \times 5 \times 5$ cm (length, width and height, respectively). Samples were immediately transported to a laboratory for petrological, mineralogical and geochemical analyses. Of these, 3 shale samples were collected from a well-exposed geological profile of the Niutitang formation in Rongxi, while the other 12 samples were obtained from fresh outcrops in Rongxi and Qingxichang (Fig. 1).

3.2. Experiments and methods

The experimental methods and criteria used in this study strictly followed the China Geological Survey Bureau standards (No. DD2006-07). The petrological, mineralogical and geochemical analyses were conducted using thin section identification (TSI), scanning electron microscopy (SEM), energy dispersive spectrometry (EDS), X-ray diffraction (XRD), X-ray fluorescence spectrometry (XRF) and inductively coupled plasma atomic emission spectrometry (ICP-OES). XRD was performed at the Chengdu Mineral Resources Administration and Testing Center using an XPERT-MPD. The TSI, SEM, EDS, XRF and ICP-OES analyses were performed at the Chongqing Mineral Resources Administration and Testing Center using a Leica DM2700P, TM 3000, S-3400N, Axios (PW4400) and iCAP 6000, respectively.

TSI and SEM were used to identify the microstructure and mineral composition, while XRD was used to quantify specific mineral contents. In addition, SEM-EDS was used to qualitatively describe crucial minerals.

XRF was used to quantify major elements, such as SiO_2 , Al_2O_3 , Fe_2O_3 and TiO_2 . In addition, trace elements and rare earth elements (REE) were quantified via ICP-OES. The trace elements discussed in this study include Th and U, while the REE include LREE, HREE, La, Yb and Ce.

To ensure the reliability of the elemental analyses, we adopted a strict error check process to ensure reliability via quality control (standard reference No. DZ0130.3–2006). Elemental testing was repeated twice for each sample. The relative deviation (RD) and permissible error (YC) were then calculated using Eqs. (1) and (2):

$$\text{RD} = (B - A) / [0.5 \times (A + B)] \times 100\% \quad (1)$$

$$\text{YC} = C \times (14.37\bar{X}^{-0.1263} - 7.659) \quad (2)$$

where A and B represent the element values that were measured twice for each sample ($\mu\text{g/g}$), \bar{X} is the average mass fraction of a composition (%) and C is the relative error coefficient for multiple analyses of any mineral composition. The value of C is 1 for major and trace elements in sedimentary samples.

According to Eqs. (1) and (2), if the value of RD is less than YC, then the element analysis results are reliable and an average value was then used, based on the repeated measurements.

4. Results and discussion

4.1. Petrography characteristics

Using the Rongxi profile in Xiushan County as an example (Fig. 1), we divided the Niutitang formation into five different sediment sections (Fig. 3). The first section is black shale with phosphate at the bottom, representing an extensive transgression. The sedimentary structure mainly consists of horizontal bedding that partially contains a pyrite strip, which suggests that an extensive water body was present during early sedimentation (Zhang et al., 2008; Yang et al., 2011). The second section is a

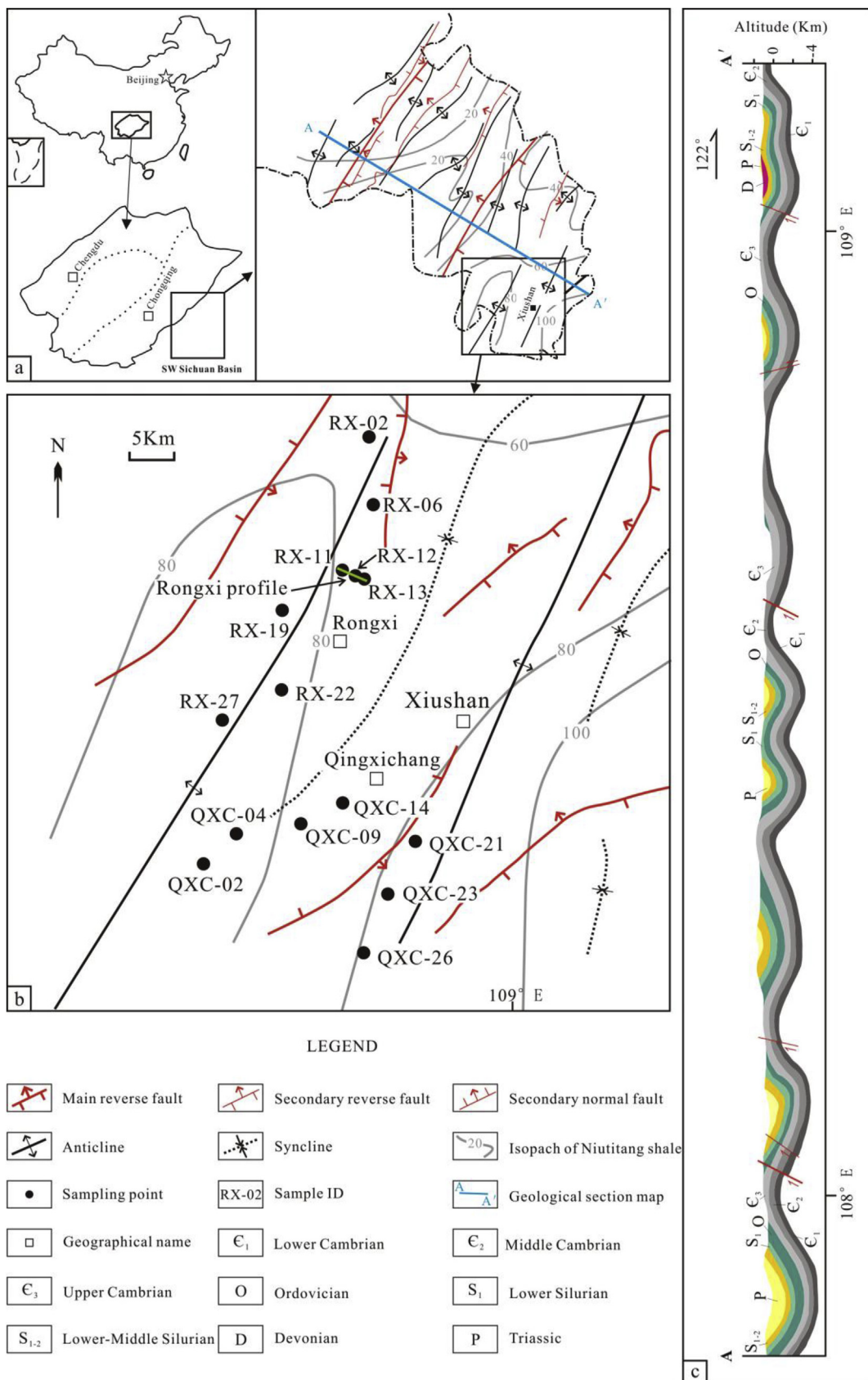


Fig. 1. Geological framework, sampling locations, and geological cross section in the southeast margin of Sichuan Basin (modified from Long et al., 2012).

System	Epoch	Formation	Thickness	Section	Lithology
Silurian	Middle-Lower	Hanjidian	200~600		Gray Sandy Dolomite
	Lower	Shiniulan	150~350		Gray Shale Mudstone Silty Mudstone
		Longmaxi	100~400		Black Carbonaceous and Siliceous Shale Gray Silty Mudstone Siltstone
	Upper	Wufeng	3~10		Black Carbonaceous and Siliceous Shale
		Dongcaogou	2~7		Gray Marlstone
		Baota	20~60		Gray Containing Biological Crumbs Limestone
Ordovician	Middle	Shizipu	10~100		Gray Containing Biological Crumbs Limestone Argillaceous Limestone
		Meitan	100~400		Gray Shale, Silty Shale Dark Gray, Argillaceous Limestone Kelly Shale, Silty Shale
	Lower	Honghuayuan	10~80		Gray Containing Biological Crumbs Limestone
		Tongzi	100~170		Gray Shale Limy Dolomite, Argillaceous Dolomite
		Loushanguan	550~650		Gray Sandy Dolomite
Cambrian	Middle	Gaotai	110~190		Gray Sandy Dolomite Shale
		Qingxudong	100~200		Gray Limestone Oolitic Limestone
	Lower	Jindingshan	115~147		Grayish-green Shale
		Mingxinsi	139~371		Grayish-green Shale Mudstone, Silty Mudstone
		Niutitang	125~481		Gray Silty Mudstone Mudstone Balck Carbonaceous and Siliceous Shale
Sinian	Upper	Dengying	537~592		Gray Dolomite
	Lower	Doushantuo	138~165		Mudstone Gray Marlstone

Fig. 2. Integrated stratigraphic column of the southeastern Sichuan basin from Sinian to Silurian.

thin-layer of grey silty mudstone with a pelitic texture and massive bedding. The third section is black carbonaceous shale with a pelitic texture and horizontal bedding, which suggests that suspended materials may have participated in the sedimentation (Hill et al., 2007b). The fourth section is grey mudstone with a thin-layered structure, horizontal bedding and undulating bedding. The fourth section also includes a locally developed sandy belt, which reflects the relatively low energy of the early aquatic environment (Hill et al., 2007b). The fifth section is dark-grey carbonaceous shale with a pelitic texture and horizontal bedding, within which banded and massive pyrites are common. In general, the Niutitang shale in the southeastern Sichuan Basin is mainly black, dark-grey through grey, indicating the shale sedimentation occurred in a mesopelagic zone reduction environment.

4.2. Mineralogy characteristics

Shale samples display specific variations in mineralogical composition. The Niutitang shale samples from the study area exhibit an intermediate combination of detrital minerals and clay minerals. The detrital minerals, such as quartz, feldspar, carbonate minerals and pyrite, comprise between 52% and 90% of the sample composition with an average of 71%. The clay minerals are composed of illite, chlorite and illite-smectite mixed-layer minerals. Detailed mineral compositions of the selected shale samples are shown in Fig. 4.

4.2.1. Quartz

The average quartz content is 44.98% and ranges between 33% and 64% (Fig. 4a). Both authigenic and epigenetic quartz is present

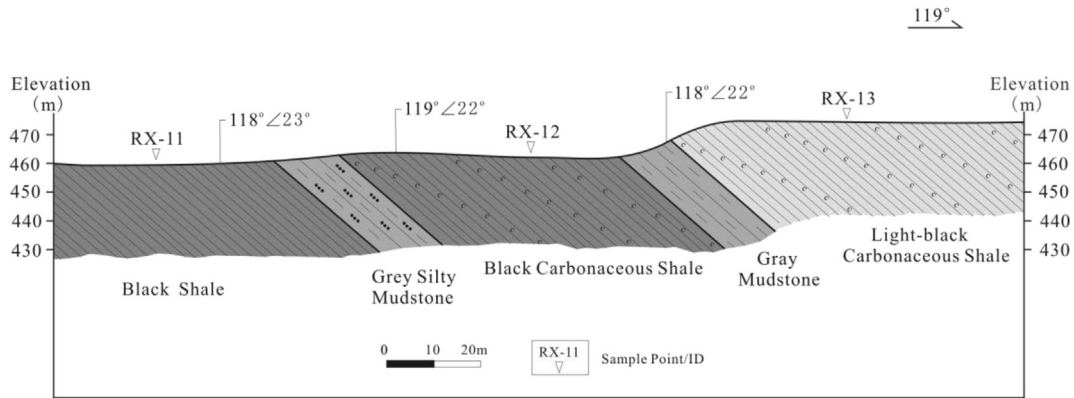


Fig. 3. Rongxi profile (Lower Cambrian Niutitang formation) in Xiushan County, southeastern Sichuan basin.

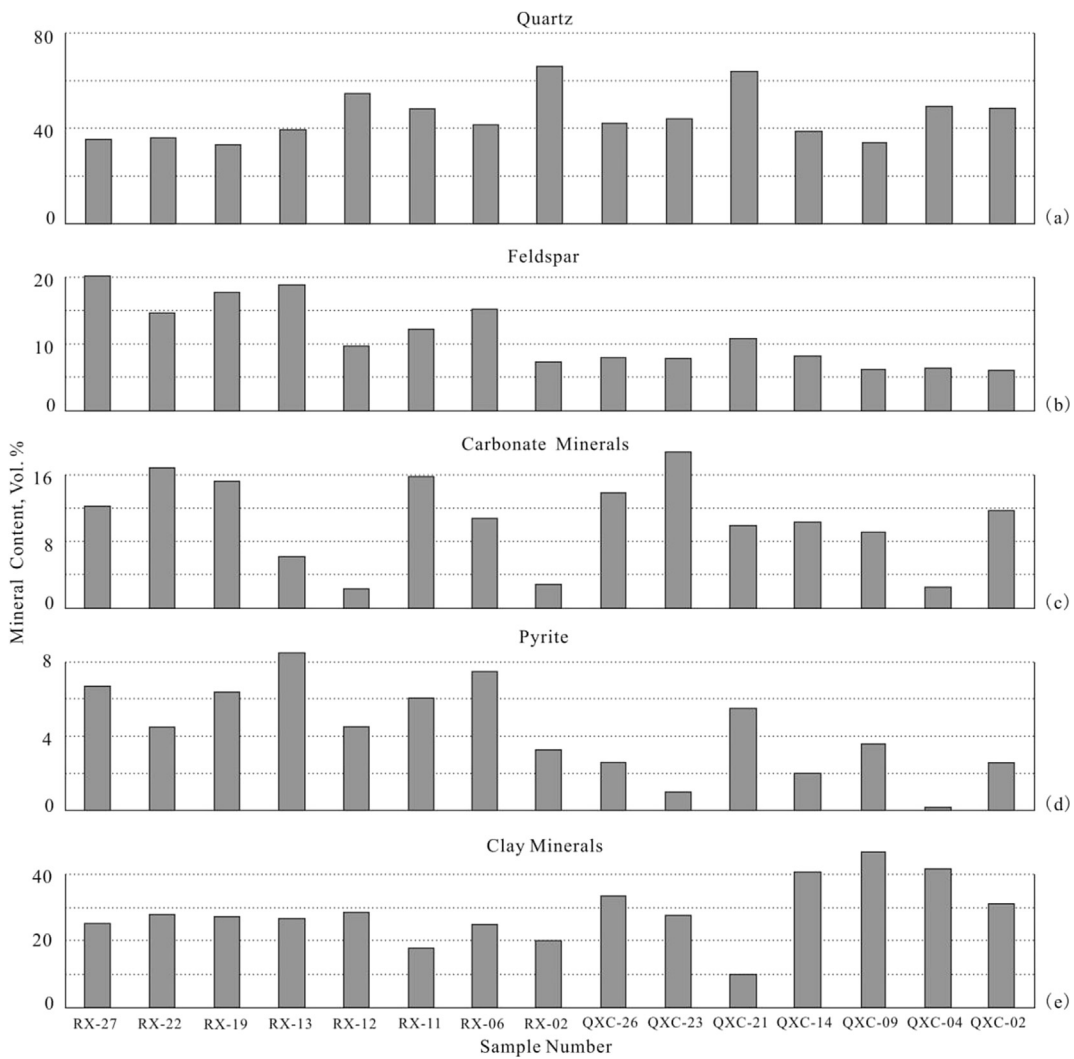


Fig. 4. The mineral compositions of the selected shale samples.

in the Niutitang shale. The authigenic quartz comprises the largest proportion and mainly exhibits a cryptocrystalline texture, which exists in both spherulitic and xenomorphic granular forms (Fig. 5a). The cryptocrystalline quartz is irregular in shape, with an average particle size $<50\text{ }\mu\text{m}$ (typically $<20\text{ }\mu\text{m}$). Tiny recrystallization quartz encases the cryptocrystalline quartz. Spherulitic and

xenomorphic quartz with both xenomorphic and columnar characteristics mainly exhibit arenaceous and hypidiomorphic textures. The average particle size of quartz with arenaceous texture is $<30\text{ }\mu\text{m}$ (typically $<20\text{ }\mu\text{m}$). Quartz with arenaceous texture is evenly distributed, with those particles present in a directional alignment (Fig. 5a). The quartz with hypidiomorphic and

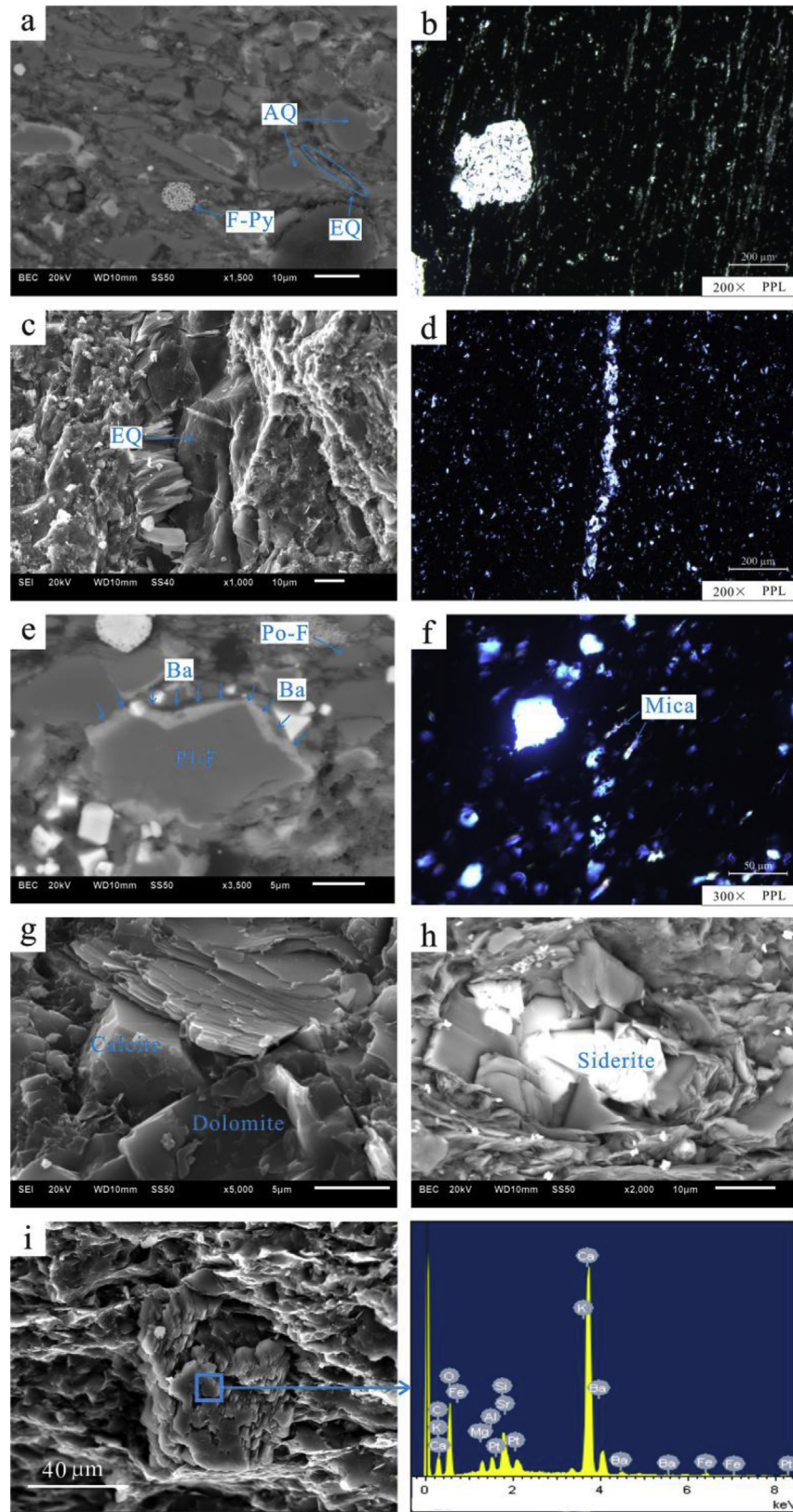


Fig. 5. Photomicrographs and SEM-EDS images of the Niutitang formation shale (AQ, authigenic quartz; EQ, epigenetic quartz; F-Py, frambooidal pyrite; Po-F, potassium feldspar; Pl-F, plagioclase feldspar; PPL, plane-polarized light). a, spherulitic, xenomorphic, granular quartzes, and frambooidal pyrite; b, quartz exhibits aggregate structures and directional alignments; c, epigenetic quartz distributed in veins with irregular shapes; d, the body of the epigenetic quartz vein; e, potassium feldspar and barium minerals; f, small amount of mica; g-h, calcite, dolomite and siderite, the main composition of carbonate minerals; and i, energy spectrum analysis for barium minerals.

xenomorphic columnar textures, which are associated with carbonate minerals, are usually presents as an aggregate structure with an average particle size of $<10 \mu\text{m}$. Some quartz samples exhibit aggregate structures and directional alignments (Fig. 5b).

The epigenetic quartz is distributed in veins with irregular shapes. Its particle size is typically larger than authigenic quartz, with an average size of $<50 \mu\text{m}$ (Fig. 5a and c). The body of the epigenetic quartz vein cuts through the authigenic quartz, and the vein body extension is consistent with the orientation of the epigenetic quartz (Fig. 5d).

4.2.2. Feldspar

Feldspar, which mainly consists of plagioclase feldspar and potassium feldspar, accounts for 6.1–20.3% of the sample composition (Fig. 4b). Potassium feldspars are randomly distributed among the plagioclase feldspars. Feldspar is uniformly distributed in rocks with arenaceous textures, and its particle size is $<50 \mu\text{m}$ (typically $<20 \mu\text{m}$) (Fig. 5e).

A limited number of samples from the Rongxi profile contain a small amount of potassium feldspar (Fig. 5e) and mica (Fig. 5f) along the cleavage planes, as well as metasomatic feldspar alterations. In addition, barium (Ba) minerals are abundant in individual samples (Fig. 5e and i).

4.2.3. Carbonate minerals

Carbonate minerals, which mainly consist of calcite (Fig. 5g), dolomite (Fig. 5g) and siderite (Fig. 5h), average 10.6% of the sample composition, ranging between 2% and 17% (Fig. 4c). The majority of the carbonate minerals exist as microcrystalline or crystalloblastic textures and are highly idiomorphic with relatively complete crystal forms. Carbonate mineral particle sizes are generally $<50 \mu\text{m}$, but individual mineral may be $>100 \mu\text{m}$. The recrystallization and overgrowths are apparent for the fine grained carbonate minerals, some of which are granular, evenly distributed and associated with quartz (Fig. 5d). In addition, coarse grain carbonate minerals develop wavy extinctions. Moreover, we observed that small amounts of carbonate minerals were directionally scattered with other associated minerals (Fig. 5b).

4.2.4. Pyrite

Pyrite, a type of authigenic mineral with an idiomorphic or hypidiomorphic granular structure, was formed during the early sedimentary period. It is the main metallic mineral of the Niutitang formation shales, as noted by macroscopic (Fig. 6a and b) and microscopic observations (Fig. 6c-f).

The pyrite content in the entire sample composition is low (4.34% on average). Two principal mineral distribution patterns were observed. One distribution occurs in black shales with vein or fine vein forms (Fig. 6a-c), in which the vein and rock stratification are always in the same direction. The pyrite vein widths vary from 10 to 1000 μm , while the particle size ranges from 10 to 100 μm . A second distribution occurs in tiny particles that are disseminated in other mineral grains (Fig. 6d-f), in which the granularity is typically $<20 \mu\text{m}$. The particle pyrites can be divided into two types: the well-formed crystalline cubic type (Fig. 6d) and the framboidal type (Fig. 6d-f and Fig. 5a).

4.2.5. Clay minerals

The clay mineral content is a key parameter in shale gas reservoirs (Ma et al., 2015). Clay minerals are always distributed in the interparticle layers of brittle minerals or rock grains with well-developed crystallinity and irregular features (Fig. 7a). However, some clay minerals exhibit a directional property (Fig. 7b).

The clay mineral content averaged 28.76% in this study, ranging from 9% to 48% of the entire sample composition (Fig. 4e). The clay

minerals are composed of illite, chlorite and illite-smectite mixed-layer minerals (I-S mixed-layer), among which illite accounts for the largest portion of the total clay mineral content (Fig. 8).

4.2.6. Mineralogical characteristics and relation to the sedimentary environment

Certain shale mineralogical characteristics can indicate specific sedimentary characteristics and regions of provenance. The detrital minerals in the study area are characterized by semicrystalline, xenomorphic and hypidiomorphic textures, with small mineral particles and medium psephicity. Moreover, the detrital mineral composition mainly consists of stable minerals, such as quartz, feldspar and carbonate minerals, while the clay mineral components are also stable and lack chalcocite clastics. These observations suggest that the majority of the unstable minerals decomposed completely during the long transport process. Thus, we speculate that the neritic zone and slope zone represent the regions of sediment provenance.

Both cubic and framboidal pyrites were found in the mineral compositions of the selected samples. According to Wilkins et al. (1996), particle of framboidal pyrite can be used to judge the reduction-oxidation conditions that occurred during the sedimentary period. The framboidal pyrite particle size typically ranged from 4 μm to 6 μm in this study, which is consistent with the framboid diameter (range between 4.8 μm and 6.1 μm) of samples from the Black Sea (Wilkins et al., 1996). Thus, we speculate that the Niutitang shales were deposited in a hydrostatic reducing environment during the sedimentary period. Furthermore, the observed enrichment in Ba may indicate that the sedimentation was influenced by submarine hydrothermal processes (Rona, 1978; Feng et al., 2007), which will be discussed later in section 4.4.

4.3. Geochemical characteristics

15 samples were analyzed for elemental compositions. The results are presented in Table 1. All measurement results passed the previously noted quality check of Eqs. (1) and (2) and met the No. DZ0130.3–2006 standard.

4.3.1. Characteristics of major elements

The major sedimentary rock elements, such as SiO_2 , Al_2O_3 , Fe_2O_3 and TiO_2 , are relatively stable and were unaffected by any late-stage diagenesis (Aitchison and Flood, 1990; Wen and Carignan, 2011). The Al_2O_3 and TiO_2 contents are mainly associated with terrigenous material inputs, while the Fe_2O_3 enrichment is due to the presence of hot waters at a mid-ocean ridge (Murray et al., 1992a,b). Murray et al. (1992a,b) and Murray (1994) created graphical models to identify sedimentary environments based on $\text{Fe}_2\text{O}_3/(100-\text{SiO}_2)$ vs. $\text{Al}_2\text{O}_3/(100-\text{SiO}_2)$ and $\text{Fe}_2\text{O}_3/\text{TiO}_2$ vs. $\text{Al}_2\text{O}_3/(\text{Al}_2\text{O}_3 + \text{Fe}_2\text{O}_3)$ relationships.

We used these relationships to plot our data on two ratio diagrams, as shown in Fig. 9. The Niutitang formation shale mineral components indicate that a continental margin environment existed in the southeastern Sichuan Basin (Fig. 9).

4.3.2. Characteristics of trace elements

This study only investigated Uranium (U) and Thorium (Th). Rona (1978) provided a relationship between U and Th that can be used to determine if sedimentation was influenced by hydrothermal processes. According to these ratios (Rona, 1978), $\text{U}/\text{Th} < 1$ may indicate a normal sedimentary process, whereas $\text{U}/\text{Th} \geq 1$ indicates the occurrence of hydrothermal processes. Similarly, Wignall (1994) established a correlation based on $\delta\text{U} = 2\text{U}/(\text{U} + \text{Th}/3)$, which can be used to determine a sedimentary environment. He

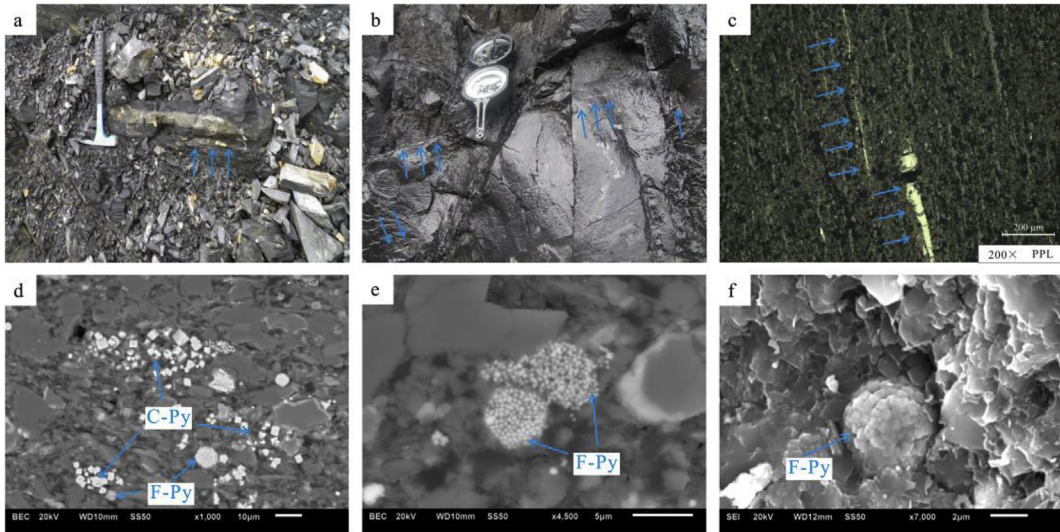


Fig. 6. Field outcrop, SEM images and photomicrograph illustrating the pyrite distribution in the Niutitang formation shales. a-b, pyrite stripe; c, disseminated pyrites, plane polarized light; d, combination of frambooidal pyrites (F-Py) and cubic pyrites (C-Py); e-f, frambooidal pyrites (F-Py).

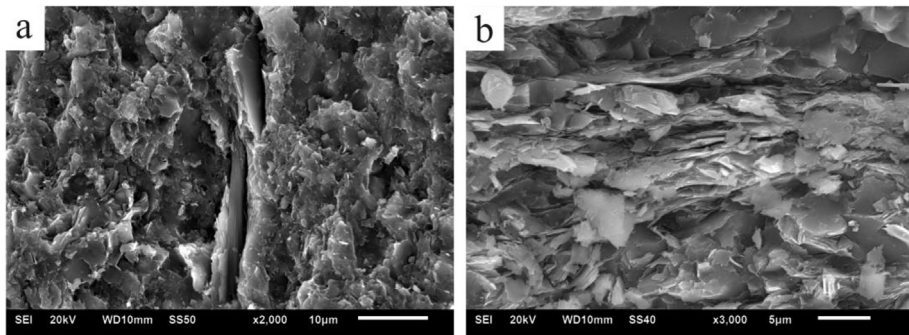


Fig. 7. SEM images of samples. a, Clay minerals with well-developed crystallinity and irregular features; b, clay minerals with directional distributions.

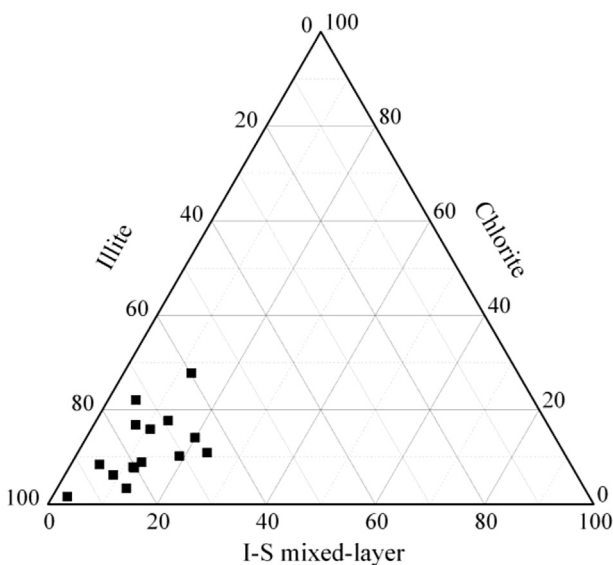


Fig. 8. Clay mineral compositions of the Niutitang formation shale.

suggested that $\delta U < 1$ indicates an oxygen-deficient environment, with $\delta U > 1$ denoting a normal seawater environment.

The trace element characteristics of U and Th are given in Table 1. The U/Th ratios are commonly < 1 , with only two exception (1.27 and 1.18). This implies that the majority of the study area represented a normal sedimentary environment. Moreover, the δU values range from 1.05 to 1.58, suggesting that the study area represented an oxygen-deficient environment during the sedimentary period.

4.3.3. Rare earth element characteristics and sedimentary environment

The geochemical behaviors of rare earth elements (REE) can provide an understanding of the geochemical processes that occurred during the period of sedimentary formation (Ruhkin and Owen, 1986; Elderfield et al., 1990; Owen et al., 1999). Allègre and Michard (1974) provided a diagram to distinguish different petrographic diageneses based on the La/Yb ratio and $\sum \text{REE}$.

We used this relationship to plot our REE content data, as shown in Fig. 10. The results show that most points fall within the area representing sedimentary rocks or the transition zone between sedimentary rocks and oceanic tholeiites, with only one point solely within the area of oceanic tholeiites. These characteristics illustrate that the bulk of the study area represented a normal sedimentary environment, with only one area affected by submarine hydrothermal processes during the sedimentary period.

In addition, δCe values reflect the enrichment and loss of cerium

Table 1

Major and trace element compositions and typical geochemical parameter characteristics of the selected shale samples.

Sample ID	Lithology (Section)	Major elements (%)			Trace elements ($\mu\text{g/g}$)			Rare earth elements ($\mu\text{g/g}$)						
		SiO ₂	Al ₂ O ₃	Fe ₂ O ₃	TiO ₂	U	Th	U/Th	δU	LREE	HREE	$\sum\text{REE}$	La/Yb	δCe
RX-27	1	57.78	12.11	5.72	0.52	2.05	5.61	0.37	1.05	141.32	38.32	179.64	11.07	0.57
RX-22	3	58.01	14.14	6.41	0.61	5.434	8.475	0.64	1.58	87.67	24.97	112.64	9.76	0.78
RX-19	4	55.51	13.64	6.22	0.58	5.191	10.18	0.51	1.21	90.21	21.08	111.29	9.64	0.67
RX-13	5	57.73	13.19	6.9	0.59	4.886	9.581	0.51	1.19	84.52	18.04	102.56	7.51	0.48
RX-12	3	59.98	12.77	5.23	0.58	4.656	9.313	0.5	1.2	87.31	18.09	105.4	8.25	0.54
RX-11	1	58.65	14.6	6.32	0.62	3.089	2.432	1.27	1.32	100.59	17.36	117.95	6.48	0.61
RX-06	1	58.21	14.39	5.46	0.6	3.684	7.25	0.51	1.21	95.05	15.41	110.46	11.11	0.57
RX-02	5	55.03	14.13	7.22	0.63	5.414	9.438	0.57	1.26	81.34	16.94	98.28	9.01	0.74
QXC-26	1	56.44	11.61	5.16	0.53	6.078	5.15	1.18	1.56	131.81	18.41	150.22	7.8	0.47
QXC-23	5	57.09	12.48	7.16	0.57	4.437	7.438	0.6	1.28	151.07	20.08	171.15	10.09	0.65
QXC-21	3	55.05	13.66	6.69	0.56	4.509	7.331	0.62	1.3	158.16	19.99	178.15	9.89	0.44
QXC-14	4	57.64	12.82	6.77	0.52	4.463	7.644	0.58	1.27	184.39	21.02	205.41	9.04	0.69
QXC-09	2	58.24	13.71	5.54	0.61	3.769	6.625	0.57	1.26	210.52	22.89	233.41	8.67	0.72
QXC-04	1	56.88	13.11	6.71	0.59	4.124	8.319	0.5	1.2	197.34	23.01	220.35	7.82	0.79
QXC-02	3	50.29	10.21	4.75	0.47	4.068	8.644	0.47	1.17	222.76	24.11	246.87	7.71	0.63

Where Section 1 represents black shale; Section 2 represents grey silty mudstone; Section 3 represents black carbonaceous shale; Section 4 represents grey mudstone; Section 5 represents dark-grey carbonaceous shale; $\delta\text{U} = 2\text{U}/(\text{U} + \text{Th}/3)$; $\delta\text{Ce} = \text{N}_{\text{Ce}}/(2\text{N}_{\text{La}} + \text{N}_{\text{Pr}})$, as directly obtained by the system, among which N_{Ce} , N_{La} and N_{Pr} are calculated from the REE chondrite-normalized North American shale composite (NASC) based on test values.

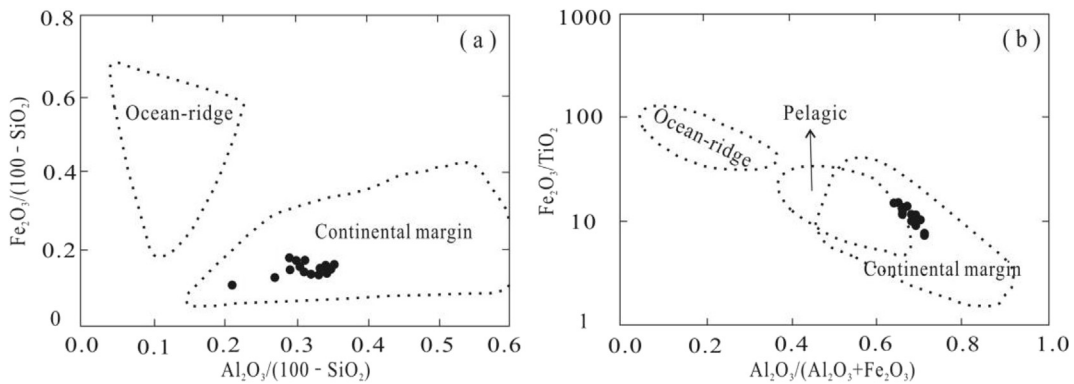
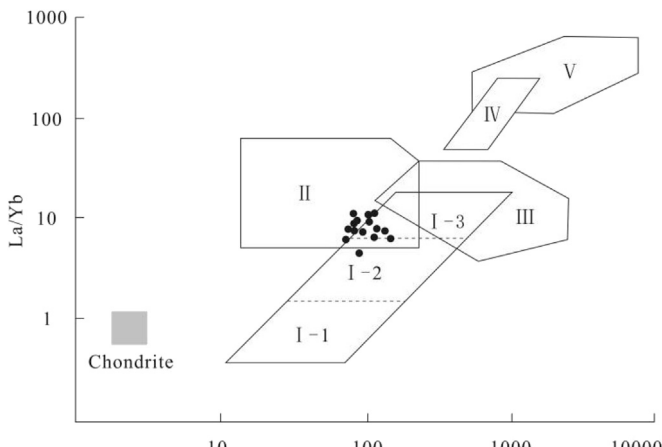


Fig. 9. Major element diagrams of the Niutitang formation shale in the southeastern Sichuan basin. a) $\text{Fe}_2\text{O}_3/(100 - \text{SiO}_2)$ vs. $\text{Al}_2\text{O}_3/(100 - \text{SiO}_2)$; b) $\text{Fe}_2\text{O}_3/\text{TiO}_2$ vs. $\text{Al}_2\text{O}_3/(\text{Al}_2\text{O}_3 + \text{Fe}_2\text{O}_3)$ (modified from Murray et al., 1992a,b; Murray, 1994).



I-1.Oceanic basalt; I-2.Continental tholeiitic; I-3.Alkalic basalt;
II.Sedimentary rocks; III.Granite; IV.Kimberlite; V.Carbonatite

Fig. 10. La/Yb vs. REE diagram of the Lower Cambrian Niutitang formation shale in southeastern Sichuan basin (modified from Allegre and Michard, 1974).

(Ce), which is particularly sensitive to variations in oxidation-deoxidization condition. Thus, the δCe index can reflect the

oxidation-reduction environment of the paleo-ocean (Hein et al., 1981). Ce includes the variable valence elements of Ce^{3+} and Ce^{4+} . Ce^{3+} could transform into Ce^{4+} in an oxidizing environment, in which the latter has difficulty in dissolving. Thus, the loss of Ce resulted in a negative Ce anomaly in the water and a positive Ce anomaly in the sediments. In contrast, if Ce was activated and released into the water in the form of Ce^{3+} in an anoxic environment, then a positive Ce anomaly would occur in sea water and a negative anomaly would occur in the sediments (Morad and Felitsyn, 2001). The δCe indexes in the investigated samples are $< 1 \mu\text{g/g}$ (Table 1), indicating that the sea water represented a reducing anoxic environment during the sedimentary period.

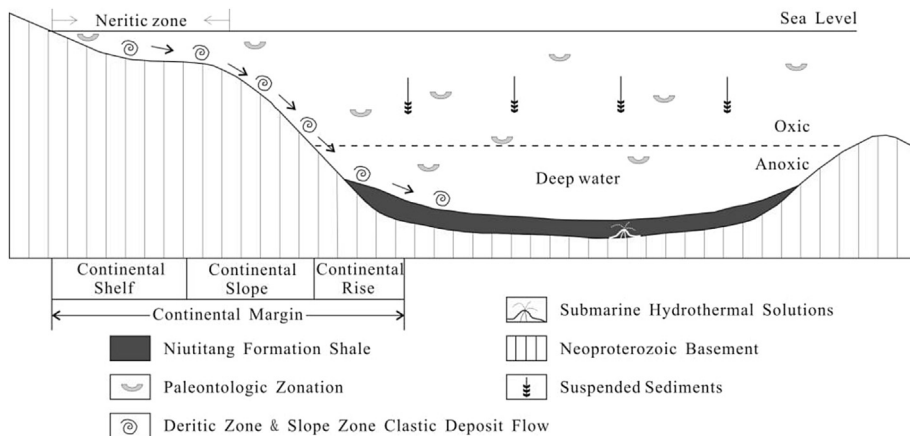
4.4. Discussion of submarine hydrothermal processes

Feng et al. (2007) indicated that submarine volcanic plumes or strong submarine hydrothermal processes may form polymetallic deposits on the seafloor. According to our field investigations, no commercial polymetallic deposits exist in the study area of the Niutitang formation. These observations indicate that the influence of submarine hydrothermal processes is local and limited to individual areas. This speculation is further confirmed by our analysis of data, which suggests that only individual samples exhibit the properties associated with hydrothermal processes (Table 1 and Fig. 10).

Table 2

Sedimentary characteristics of Niutitang shales and available proofs.

Sedimentary characteristics and environment	Available proofs
Sedimentary hydrogeology and hydrodynamics	Weak hydrodynamic, deep water, oxygen-deficient reducing environment Certain content of suspended sediments
Sediment sources	Linking to neritic and continental slope zones
Other sedimentary characteristics	Locally isolated areas affected by submarine hydrothermal sedimentation

**Fig. 11.** Sedimentary pattern of the Lower Cambrian Niutitang formation shale in southeastern Sichuan basin.

Submarine hydrothermal processes may significantly impact various shale gas reservoir characteristics, such as the mineral composition, the maturity of the organic matter and resulting porosity or permeability variations. Further research is required to determine the specific impacts of the submarine hydrothermal processes on the shale gas reservoir of the Niutitang formation in the southeastern Sichuan basin.

5. Conclusions

According to petrological, mineralogical and geochemical analyses of 15 shale samples from the Lower Cambrian Niutitang formation in the southeast margin of Sichuan Basin, we summarize the sedimentary characteristics and environment of the Niutitang shale in Table 2 and Fig. 11. The following conclusions were made:

The development of horizontal bedding, the existence of frambooidal pyrite, $\delta\text{U} \geq 1$ and the negative δCe index anomaly illustrate that sedimentation of the Niutitang shale formation occurred in a weak hydrodynamic, deep water, oxygen-deficient reducing environment.

The properties of the detrital mineral and analyses of the major elements indicate that the geotectonic background of the Niutitang shale formation can be linked to the neritic and continental slope zones. The development of horizontal bedding indicates that suspended sediments participated in the sedimentation.

The presence of Ba minerals, REE characteristics and the trace element (U/Th) index indicate that the majority of the study area represented a normal sedimentary environment, but several isolated areas were affected by submarine hydrothermal sedimentation.

The sedimentation of the Niutitang shale formation likely occurred in a weak hydrodynamic, deep water, oxygen-deficient reducing environment (Fig. 11). The major sediment sources are continental margins, such as the neritic or continental slope zones. Some suspended sediments were involved in the sedimentary

process. In local areas, the sedimentary process was affected by submarine hydrothermal activities.

Acknowledgments

We acknowledge financial support from the CNPC Innovation Foundation (2014D-5006-0102), the Foundation for the Author of National Excellent Doctoral Dissertation of PR China (201253) and the National Natural Science Foundation of China (41302104). This study would not have been possible without the assistance of the Chongqing Institute of Geology and Mineral Resources, especially their support of our field work, geological sampling and experimental analyses.

References

- Aitchison, J.C., Flood, P.G., 1990. Geochemical constraints on the depositional setting of Palaeozoic cherts from the New England orogen, NSW, eastern Australia. *Mar. Geol.* 94 (2), 79–95.
- Allègre, C.J., Michard, G., 1974. *Introduction to Geochemistry (Geophysics and Astrophysics Monographs)*, vol. 10. D. Reidel Publishing Company, Boston, USA.
- Arthur, M.A., Sageman, B.B., 1994. Marine black shales: depositional mechanism and environments of ancient deposits. *Annu. Rev. Earth Planet. Sci.* 22, 499–551.
- Chalmers, G.R.L., Ross, D.J.K., Bustin, R.M., 2012. Geological controls on matrix permeability of Devonian gas shales in the Horn river and liard basins, north-eastern British Columbia, Canada. *Int. J. Coal Geol.* 103, 120–131.
- Chen, L., Lu, Y., Jiang, S., Li, J., Guo, T., Luo, C., Xing, F., 2015a. Sequence stratigraphy and its application in marine shale gas exploration: a case study of the Lower Silurian Longmaxi Formation in the Jiaoshiba shale gas field and its adjacent area in southeast Sichuan Basin, SW China. *J. Nat. Gas. Sci. Eng.* 27, 410–423.
- Chen, L., Lu, Y.C., Jiang, S., Li, J.Q., Guo, T.L., Luo, C., 2015b. Heterogeneity of the lower Silurian Longmaxi marine shale in the southeast Sichuan basin of China. *Mar. Pet. Geol.* 65, 232–246.
- Crutis, J.B., 2002. Fractures shale-gas system. *AAPG Bull.* 86, 1921–1938.
- Dong, D.Z., Cheng, K.M., Wang, Y.M., 2010. Forming conditions and characteristics of shale gas in the lower paleozoic of the upper Yangtze region, China. *Oil Gas. Geol.* 31 (3), 288–308 (in Chinese with English abstract).
- EIA (Energy Information Administration), U. S., 2014. Shale Gas Provides Largest Share of U.S. Natural Gas Production in 2013. November 25. <http://www.eia.gov/todayinenergy/detail.cfm?id=18951>.
- Elderfield, H., Goddard, R.U., Sholkovitz, E.R., 1990. The rare earth elements in rivers,

- estuaries and coastal sea and their significance to the composition of ocean water. *Geochim. Cosmochim. Acta* 54, 971–991.
- Feng, S.B., Xing, K., Zhou, H.H., Yan, C.H., Peng, Y., Zhao, J.M., Hu, S.B., Ren, J.G., 2007. Geochemical characteristics of hydrothermal sediments for baritic rocks of Erlangping Group in northern Qinling Mountains and their significance for mineralization. *Glob. Geol.* 26 (2), 199–206 (in Chinese with English abstract).
- Hao, F., Zou, H.Y., Lu, Y.C., 2013. Mechanisms of shale gas storage: implications for shale gas exploration in China. *AAPG Bull.* 97, 1325–1346.
- Hein, J.R., Vallier, T.L., Allan, M.A., 1981. Chert petrology and geochemistry, mid-Pacific mountains and Hess rise, deep sea drilling project leg 62. *Deep Sea Drill. Proj. Rep. Publ.* 62, 711–748.
- Hill, R.J., Jarvie, D.M., Zumberge, J., Henry, M., Pollastro, R.M., 2007a. Oil and gas geochemistry and petroleum systems of the Fort Worth Basin. *AAPG Bull.* 91, 445–473.
- Hill, R.J., Zhang, E.T., Katz, B.J., Tang, Y.C., 2007b. Modelling of gas generation from the Barnett shale, Fort Worth basin. *Tex. AAPG Bull.* 91, 501–521.
- Huang, J.L., Zou, C.N., Li, J.Z., Dong, D.Z., Wang, S.J., Wang, S.Q., Cheng, K.M., 2012. Shale gas generation and potential of the lower Cambrian Qiongzhusi Formation in the southern Sichuan basin, China. *Pet. Explor. Dev.* 39 (1), 75–81 (in Chinese with English abstract).
- Jarvie, D.M., Hill, R.J., Ruble, T.E., Pollastro, R.M., 2007. Unconventional shale-gas system: the Mississippian Barnett Shale of north-central Texas as one model for thermogenic shale-gas assessment. *AAPG Bull.* 91, 475–499.
- Jiang, Z.X., Guo, L., Liang, C., 2013. Lithofacies and sedimentary characteristics of the Silurian Longmaxi shale in the southeastern Sichuan basin, China. *J. Palaeogeogr.* 2 (3), 238–251.
- Johnson, C., Boersma, T., 2013. Energy (in) security in Poland the case of shale gas. *Energy Policy* 53, 389–399.
- Long, P.Y., Zhang, J.C., Jiang, W.L., Nie, H.K., Tang, X., Han, S.B., Xing, Y.W., 2012. Analysis on pores forming features and its influence factors of reservoir well Yuye-1. *J. Cent. South Univ. Sci. Technol.* 43 (10), 3954–3963 (in Chinese with English abstract).
- Ma, Y., Zhong, N.N., Li, D.H., Pan, Z.J., Cheng, L.J., Liu, K.Y., 2015. Organic matter/clay mineral intergranular pores in the Lower Cambrian Lujiaoping Shale in the north-eastern part of the upper Yangtze area, China: a possible microscopic mechanism for gas preservation. *Int. J. Coal Geol.* 137, 38–54.
- Morad, S., Felitsyn, S., 2001. Identification of primary Ce-anomaly signatures in fossil biogenic apatite: implication for the Cambrian oceanic anoxia and phosphogenesis. *Sediment. Geol.* 143, 259–264.
- Murray, R.W., 1994. Chemical criteria to identify the deposition environment of chert: general principles and applications. *Sediment. Geol.* 90, 213–232.
- Murray, R.W., Buchholtz Ten Brink, M.R., Gerlach, D.C., 1992a. Rare earth, major, and trace element composition of Monterey and DSDP chert and associated host sediment: assessing the influence of chemical fractionation during diagenesis. *Geochim. Cosmochim. Acta* 56 (7), 2657–2671.
- Murray, R.W., Jone, D.L., Buchholtz Ten Brink, M.R., 1992b. Diagenetic formation of bedded chert: evidence from chemistry of the chert-shale couplet. *Geology* 20, 271–274.
- Nie, H.K., Zhang, J.C., Li, Y.X., 2011. Accumulation conditions of the lower Cambrian shale gas in the Sichuan basin and its periphery. *Acta Pet. Sin.* 32 (6), 959–967 (in Chinese with English abstract).
- Owen, A.W., Armstrong, H.A., Floyd, J.D., 1999. Rare earth element geochemistry of upper Ordovician cherts from the southern upland of Scotland. *J. Geol. Soc.* 156, 191–204.
- Reinhardt, J.W., 1988. Uppermost Permian reefs and Permo-Triassic sedimentary facies from the southeastern margin of Sichuan basin, China. *Facies* 18, 231–288.
- Rona, P.A., 1978. Criteria for recognition of hydrothermal mineral deposits in ocean crust. *Econ. Geol.* 73 (2), 135–160.
- Ruhkin, D.E., Owen, R.M., 1986. The rare earth element geochemistry of hydrothermal sediments from the East Pacific Rise: examination of a seawater scavenging mechanism. *Geochim. Cosmochim. Acta* 50, 393–400.
- Wang, S.Q., Chen, G.S., Dong, D.Z., 2009. Accumulation conditions and exploitation prospect of shale gas in the lower Paleozoic Sichuan basin. *Nat. Gas. Ind.* 29 (5), 51–58 (in Chinese with English abstract).
- Wen, H.J., Carignan, J., 2011. Selenium isotopes trace the source and redox processes in the black shale-hosted Se-rich deposits in China. *Geochim. Cosmochim. Acta* 75, 1411–1427.
- Wignall, P.B., 1994. Black Shales. Oxford University Press, Oxford.
- Wilkins, R.T., Barnes, H.L., Barantley, S.L., 1996. The size distribution of framboidal pyrite in modern sediments: an indicator of redox conditions. *Geochim. Cosmochim. Acta* 60 (20), 3897–3912.
- Wu, J., Yu, B., Zhang, J., Li, Y., 2013. Pore characteristics and controlling factors in the organic-rich shale of the Lower Silurian Longmaxi formation revealed by samples from a well in southeastern Chongqing. *J. Front. Earth Sci. China* 20 (3), 260–269.
- Xie, C., Zhang, J.C., Li, Y.X., Wang, X.H., 2013. Characteristics and gas content of the lower Cambrian dark shale in well Yuke-1, southeast Chongqing. *Oil Gas. Geol.* 34, 11–15 (in Chinese with English abstract).
- Xue, H., Jiang, P., Xu, R., Zhao, B., Zhou, S., 2016. Characterization of the reservoir in lower Silurian and lower Cambrian shale of south Sichuan basin, China. *J. Nat. Gas. Sci. Eng.* 29, 150–159.
- Yang, F., Ning, Z.F., Zhang, R., Zhao, H.W., Krooss, B.M., 2015. Investigations on the methane sorption capacity of marine shales from Sichuan Basin, China. *Int. J. Coal Geol.* 146, 107–117.
- Yang, X., Liu, X.W., Wang, Y.D., Liu, Y.H., Zheng, J.J., 2011. The tectonic controls on the distribution of marine oil and gas in the adjacent area of Xuefeng mountain. *J. Southwest Pet. Univ. Sci. Technol. Ed.* 33 (4), 7–12.
- Zeng, L.B., Lyu, W.Y., Li, J., Zhu, L.F., Weng, J.Q., Yue, F., Zu, K.W., 2016. Natural fractures and their influence on shale gas enrichment in Sichuan Basin, China. *J. Nat. Gas. Sci. Eng.* 30, 1–9.
- Zhang, J.C., Nie, H.K., Xu, B., Jiang, S.L., Zhang, P.X., Wang, Z.Y., 2008. Geological condition of shale gas accumulation in Sichuan Basin. *Nat. Gas. Ind.* 28, 151–156 (in Chinese with English abstract).